Synchronization of Mutually Coupled Digital PLLs in Massive MIMO Systems

David J. Jörg*‡, Alexandros Pollakis†‡, Lucas Wetzel*‡, Marvin Dropp†, Wolfgang Rave†‡, Frank Jülicher*‡, and Gerhard Fettweis†‡
*Max Planck Institute for the Physics of Complex Systems, Dresden, Germany
†Technische Universität Dresden, Vodafone Chair, Dresden, Germany
‡Center for Advancing Electronics Dresden cfAED, Dresden, Germany

***Abstract*—For next-generation wireless networks, massive multiple-input multiple-output (MIMO) promises significant performance gains compared to today's wireless communication standards. In this paper, we address the challenge of how to synchronize the carrier signals of all antenna units in a large network. We show that mutually coupled digital phase-locked loops (DPLLs) can enable in-phase synchronous clocking in large-scale systems with transmission delay. Using a phase model of coupled DPLLs including signal filtering and signal transmission delays, we show how the collective frequency and the time scales of synchronization depend on system specifications. To test our theoretical predictions, we designed and carried out experiments, thereby providing a proof-of-principle that mutually delay-coupled DPLLs can provide self-organized synchronous clocking.**

I. Introduction

In wireless communication research the multiple-input multiple-output (MIMO) concept has recently attracted attention and has found its way into modern wireless communication standards such as Long-Term Evolution (LTE) [1] and IEEE 802.11n (WiFi) [2]. MIMO relies on multiple transmission antennas operating in parallel, which use the characteristics of the different spatial transmission paths to establish orthogonal transmission channels. This concept can be exploited beneficially in terms of data rate, reliability, energy efficiency and interference handling [3]. These benefits scale with the number of antennas within the system. However, modern wireless communication standards support only a small number of antennas. Even though LTE supports up to eight antenna ports per base station, this potential is not fully exploited nowadays. Increasing the number of antennas by several orders of magnitude (massive MIMO), the benefits of conventional MIMO could be exploited on much larger scales [4], [5]. However, how to efficiently transmit data through such a large number of antennas is still an emerging research field. In large antenna systems, one major challenge is to ensure phase synchrony of the carrier signals for all antennas [6]–[9]. Hence, precise and robust clock synchronization between antenna units emerges as a critical factor, especially in distributed modular architectures [10].

Traditional clock distribution concepts rely on a single master node distributing a clocking signal through a tree-like structure to multiple slave nodes. Such structures become space and energy inefficient with an increasing system size [11], [12]. In addition, such clock trees are vulnerable to errors due to noise and cross-talk. Traditional clock distribution concepts reach their limits at the large scales that massive MIMO aims for. Hence, novel clocking concepts are required.

Clock distribution and synchronization of large scale systems is not restricted to the topic of wireless communication or engineering. In biological physics, systems exhibiting self-organized synchronization such as neuron clusters, coupled genetic oscillators, pacemaker cells in the heart, and flashing fireflies have attracted a wide experimental and theoretical research interest [13]–[15]. Through mutual coupling of their oscillatory dynamics, these systems are able to synchronize robustly and in highly noisy environments in the absence of an entraining master clock. Coupled biological oscillators can thus provide a source of inspiration for clock distribution strategies to synchronize, e.g., antenna units of a massive MIMO system. Instead of a hierarchical clock tree, where a master clock entrains each slave, we propose a network of mutually coupled clocks that are able to synchronize their clock signals in a self-organized way. For frequencies in the MHz and GHz range, common in modern electronics, the spatial distances between nodes induce transmission delays of the order of an oscillation period of the clocking signal. For instance, the typical spacing of antennas in multi-antenna arrays will lead to a transmission delay on the order of half an oscillation period. This raises the question how synchronization can be achieved in such networks in the presence of transmission delays.

In previous work, we presented a system architecture able to obtain global synchrony in large systems of analogue phase-locked loops [16]. In this paper, we extend our work to include digital phase-locked loops (DPLLs) [17]. In Section II, we develop a phase model of N mutually delay-coupled DPLLs. In Section III, in-phase synchronized solutions and their stability for networks of mutually coupled DPLLs are investigated. In Section IV, we present experimental data for two mutually coupled DPLLs and discuss measurements and theoretical results. Finally, conclusions are drawn in Section V.

II. Phase Model

The basic element of our clocking network is a digital phase-locked loop (DPLL). DPLLs are electronic clocking circuits able to synchronize their output signal to an input signal. They are commonly used in electronic system design for a wide range of clocking applications, e.g., wireless transceivers and Multiprocessor System-On-Chips. A DPLL consists of three essential functional blocks (Fig. 1): the phase detector (PD), the loop filter (LF) and the voltage-controlled oscillator (VCO). The PD is implemented as an XOR gate and compares

978-1-4673-6432-4/15/$31.00 ©2015 IEEE

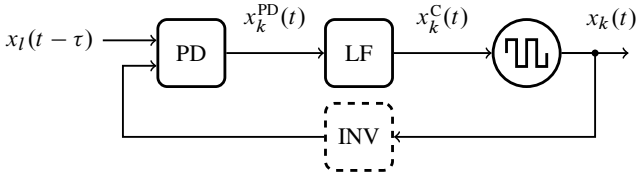

Fig. 1: Signal flow model of a PLL. The delayed input signal to PLL k is denoted by $x_l(t-\tau)$ and its output signal by $x_k(t)$. The output signal at the phase detector (PD) is denoted by $x_k^{\mathrm{PD}}(t)$ and the output signal at the loop filter (LF) by $x_k^{\mathrm{C}}(t)$. The output signal $x_k(t)$ is generated by a voltage-controlled oscillator (VCO) and fed back to the PD. A signal inverter (INV) is placed in this feedback loop which can be activated as needed.

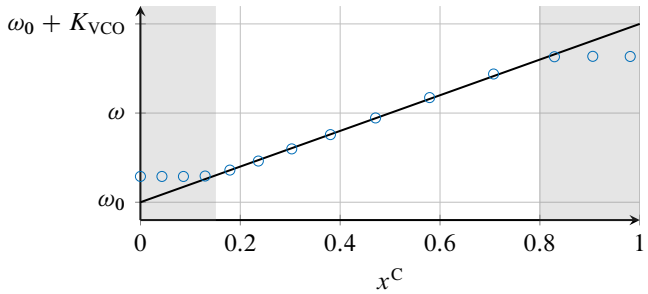

Fig. 2: Dynamic frequency of the VCO in response to an external control voltage x^{C}: linear approximation used in Eq. (4) (solid curve), measured VCO response curve from the DPLLs in our experimental setup (circles). The shaded areas display the VCO clipping region.

the external signal x_l to the feedback signal x_k. The LF is a low-pass filter that damps high frequency components of the PD's output signal x_k^{PD} and yields a control signal x_k^{C} for the VCO. The control signal x_k^{C} modulates the VCO's frequency and results in an entrainment to the input signal's phase and frequency. A signal inverter (INV) is placed within the feedback loop between the VCO and the PD, which can be used to enable an in-phase synchronized state for arbitrary transmission delay (Fig. 1), see Section IV. To develop a phase model for networks of mutually coupled DPLLs we first show the derivation for a single DPLL. Subsequently, we extend the model to a network of N coupled DPLLs. In contrast to Ref. [16], we consider digital PLLs throughout our work, implying time-continuous binary signals.

A. Coupling of a digital PLL to an external signal

The VCO outputs a rectangular oscillation with amplitude 1,

$$x_k(t) = \Pi(\phi_k(t)) \ , \tag{1}$$

where $\Pi(\phi)$ is a square-wave function, which takes the value 1 for $0 \le \phi < \pi$, the value 0 for $\pi \le \phi < 2\pi$ and satisfies $\Pi(\phi + 2\pi) = \Pi(\phi)$ for all ϕ, and $\phi_k(t)$ is the phase of oscillator k. The PD compares the external input signal x_l with the signal of the internal feedback x_k using an XOR operation. We account for transmission delays with a discrete delay τ in the input signal,

$$\begin{aligned} x_k^{\mathrm{PD}}(t) &= x_l(t-\tau) \oplus x_k(t) \\ &= x_l(t-\tau)\cdot\neg x_k(t) + \neg x_l(t-\tau)\cdot x_k(t) \ , \end{aligned} \tag{2}$$

where $\oplus$ denotes the XOR operation and $\neg x(t) = 1 - x(t)$. The PD's output signal $x_k^{\mathrm{PD}}(t)$ is filtered by the LF whose output signal x_k^{C} is given by

$$x_k^{\mathrm{C}}(t) = \int_0^\infty \mathrm{d}u \ p(u) x_k^{\mathrm{PD}}(t-u) \ , \tag{3}$$

where $p(u)$ denotes the impulse response of the LF and satisfies $\int_0^\infty \mathrm{d}u \ p(u) = 1$. The control signal $x_k^{\mathrm{C}}(t)$ is fed into the VCO and determines the VCO's oscillation frequency according to

$$\dot{\phi}_k(t) = \omega_0 + K_{\mathrm{VCO}} x_k^{\mathrm{C}}(t) \tag{4}$$

where ω_0 is the minimal frequency of the VCO for zero input and K_{VCO} is its sensitivity. We here assume that the frequency response of the VCO is linear, that is, proportional to the control signal x_k^{C}. Fig. 2 shows this linear response approximation together with the measured response curve from our experimental setup, discussed in Section IV. We consider an ideal loop filter, perfectly damping high frequency components, see Appendix. Using Eqs. (2) and (3) in Eq. (4), we obtain

$$\dot{\phi}_k(t) \simeq \omega + K \int_0^\infty \mathrm{d}u \ p(u) \, \Delta\big(\phi_l(t-\tau-u) - \phi_k(t-u)\big) \tag{5}$$

where Δ is the triangle function defined by $\Delta(\phi) = 2|\phi|/\pi - 1$ in the range $-\pi \le \phi \le \pi$ and satisfies $\Delta(\phi + 2\pi) = \Delta(\phi)$ for all ϕ, and we have defined $\omega = \omega_0 + K_{\mathrm{VCO}}/2$ and $K = K_{\mathrm{VCO}}/2$.

B. Networks of mutually coupled DPLLs

We extend the phase model for two coupled DPLLs, Eq. (5), to networks of N mutually coupled DPLLs with transmission delays. For more than one input signal to a DPLL, each input signal has to undergo the XOR operation with the feedback signal individually. The resulting signals are then averaged (Fig. 3). The phase model for N coupled DPLLs with identical intrinsic frequencies and transmission delays reads

$$\begin{aligned} \dot{\phi}_k(t) \simeq \omega + \frac{K}{n(k)} \sum_{l=1}^{N} c_{kl} \int_0^\infty \mathrm{d}u \ p(u) \\ \times \Delta\big(\phi_l(t-\tau-u) - \phi_k(t-u)\big) \ . \end{aligned} \tag{6}$$

The connections between DPLLs are described by the coupling matrix (c_{kl}) with $c_{kl} \in \{1, 0\}$, where $c_{kl} = 1$ indicates a connection between DPLL k and DPLL l. The coupling strength is normalized by the number of input signals, $n(k) = \sum_l c_{kl}$. Eqs. (6) describe a network of N coupled DPLLs, taking explicitly into account a filter impulse response $p(u)$ and identical transmission delays τ. Identical transmission delays can, e.g., be achieved in a regular square lattice with nearest-neighbor coupling.

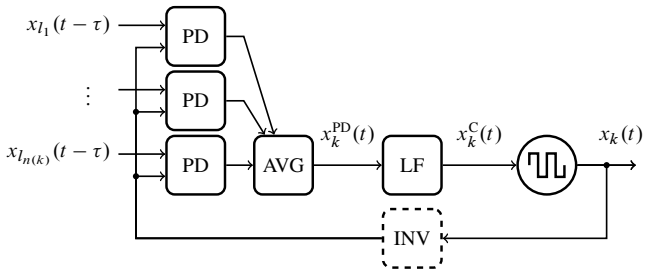

Fig. 3: Signal flow of a PLL with multiple delayed input signals. Each input signal x_{l_i} $(i = 1, \ldots, n(k))$ undergoes the XOR operation with the feedback signal individually. The resulting signals are averaged (AVG).

III. In-phase synchronized states

In massive MIMO systems, it is important that the carrier signals of all antennas are in synchrony. However, networks of mutually coupled DPLLs may also exhibit other dynamical states. Here, we analyze the existence and the stability of an in-phase synchronized state.

A. Existence of the in-phase synchronized state

The globally in-phase synchronized state is characterized by all DPLLs evolving with the same collective frequency Ω and no phase lag relative to each other,

$$\phi_k(t) = \Omega t \ . \tag{7}$$

Substituting the ansatz Eq. (7) into Eq. (6) we find

$$\Omega = \omega + K\Delta(\Omega\tau) \tag{8}$$

where we have used $\int_0^\infty \mathrm{d}u\, p(u) = 1$, $n(k) = \sum_l c_{kl}$, and the fact that Δ is even. The in-phase synchronized state exists if Eq. (8) has a solution in Ω. This solution is independent of the number N of oscillators. Depending on the value of the transmission delay τ, Eq. (8) can have multiple solutions representing different in-phase synchronized states with different collective frequencies. In the following section, we analyze the stability of these states.

B. Linear stability of the in-phase synchronized state

Whether an in-phase synchronized state can be achieved depends on its stability properties. We assess the stability of the state Eq. (8) by performing a linear stability analysis [18], [19]. We use the ansatz

$$\phi_k(t) = \Omega t + \varepsilon q_k(t) \tag{9}$$

where q_k is a perturbation of order unity to the in-phase synchronized state and ε is a small expansion parameter. The linear dynamics of the perturbation is obtained by expanding Eq. (6) to first order in ε at $\varepsilon = 0$,

$$\dot{q}_k(t) = \frac{\alpha}{n(k)} \sum_{l=1}^{N} c_{kl} \int_0^\infty \mathrm{d}u\, p(u)\big[q_l(t-\tau-u) - q_k(t-u)\big] \tag{10}$$

where

$$\alpha = K \frac{\mathrm{d}\Delta}{\mathrm{d}\phi}\bigg|_{\phi=-\Omega\tau} \ . \tag{11}$$

Note that Δ is not differentiable for arguments $m\pi$ with $m \in \mathbb{Z}$. However, $\Omega\tau$ attains such values only within the VCO clipping regions, whose description is outside the scope of our theory (see, e.g., Fig. 5). Substituting the exponential ansatz $q_k(t) = v_k e^{\lambda t}$ with $\lambda \in \mathbb{C}$ into Eq. (10) we obtain the characteristic equation

$$\lambda v_k = \alpha\, \hat{p}(\lambda) \sum_{l=1}^{N} d_{kl}(v_l e^{-\lambda\tau} - v_k) \tag{12}$$

where $\hat{p}(\lambda) = \int_0^\infty \mathrm{d}u\, \mathrm{e}^{\lambda u} p(u)$ is the transfer function of the LF and $d_{kl} = c_{kl}/n(k)$ are the components of the normalized coupling matrix $\mathbb{D} = (d_{kl})$. The in-phase synchronized state Eq. (7) is linearly stable if and only if $\mathrm{Re}(\lambda) < 0$ for all solutions to Eq. (12). The time evolution of the perturbation is dominated by the solution λ_0 with the largest real part [16], whose real part and imaginary part we denote by

$$\lambda_0 = \sigma + \mathrm{i}\beta \ , \tag{13}$$

where σ is the perturbation response rate. The imaginary part β is a frequency that modulates the collective frequency Ω [16].

The transfer function of a large class of loop filters is given by

$$\hat{p}(\lambda) = \frac{1}{(1+\lambda b)^a} \tag{14}$$

where b denotes the time constant and a the order of the filter, which set the cutoff frequency ω_c of the filter according to $\omega_\mathrm{c} = (ab)^{-1}$ [16], [20]. Substituting Eq. (14) into Eq. (12), rewriting the equation in vector form and solving the eigenvalue problem $\zeta\mathbf{v} = \mathbb{D}\mathbf{v}$, with $\mathbf{v} = (v_1, \ldots, v_N)$, we find

$$\lambda(1+\lambda b)^a + \alpha(1 - \zeta e^{-\lambda\tau}) = 0 \ . \tag{15}$$

TABLE I: Parameters of the experimental setup.

	$\omega/2\pi$	$K_\mathrm{VCO}/2\pi$
DPLL #1	1008 Hz	816 Hz
DPLL #2	1011 Hz	813 Hz
Average	1009.5 Hz	814.5 Hz
Standard deviation	0.21 %	0.26 %

Filter cutoff frequency $\omega_\mathrm{c}/2\pi$	14 Hz
Filter order a	1

TABLE II: Measurement parameters of the experiments.

description	value
signal amplitudes	5 V
sampling interval	10 µs
number of samples	109 224
FFT size	131 072
FFT frequency resolution	0.7198 Hz

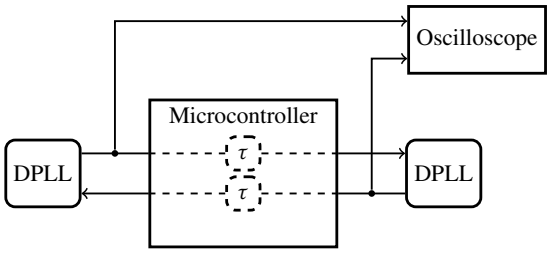

Fig. 4: Experimental setup: Two DPLLs coupled through a microcontroller, which artificially introduces a coupling delay. An oscilloscope samples the periodic signals of the DPLLs.

Eq. (15) can have multiple solutions for each ζ. Although the collective frequency Ω of the in-phase synchronized state is independent of the coupling topology as well as the properties of the LF, the linear stability is not.

IV. Measurements on a Prototype System

To test the predictions of our phase model in a real system, we conducted experiments with mutually coupled DPLLs to study their synchronization behavior. Our setup consisted of two DPLLs (CD4046B [21], specifications given in Table I), a Digilent ChipKit Max32 microcontroller [22], and a PicoScope 2205 Mixed-Signal oscilloscope [23] (Fig. 4). As electronic signals are transmitted with about two thirds of the speed of light [11], the wiring distance needed to obtain significant transmission delays in devices operating in the GHz range is of the order of centimeters, while in the kHz range, it is of the order of kilometers. Since it is technically challenging to sample signals in the GHz range, we used DPLLs that operate in the kHz regime. To achieve a significant coupling delay, we used a microcontroller that introduces the necessary delays artificially by holding back the signals for a prescribed amount of time. We used the oscilloscope to measure the DPLL's output signals (measurement parameters given in Table II). From these signals, we extracted a phase time series from which we obtained (i) the exponential relaxation time to the synchronized state and (ii) the collective frequency of the DPLLs once the synchronized state was reached.

Fig. 5 shows the measurements of the collective frequency Ω of the in-phase synchronized state for different values of the coupling delay, together with the results from the phase model, Eq. (8). In addition to the in-phase synchronized state discussed in Sec. III-A, the system of two DPLLs also exhibits an anti-phase synchronized state, characterized by $\phi_1(t) = \phi_2(t) - \pi$. In the phase model, the collective frequency of the anti-phase state can be obtained as $\Omega = \omega - K\Delta(\Omega\tau)$; note the inverted sign compared to Eq. (8). The system considered here exhibits bistability of both solutions in certain regions in parameter space. Moreover, above a certain value of the transmission delay, the system exhibits multiple in-phase and/or anti-phase synchronized states with different collective frequencies. To obtain the frequency of all solutions, the system has to be prepared in different initial conditions. Outside the VCO clipping regions, the measurements are in excellent agreement with the theoretical results from the phase model. In the VCO clipping regions, the linear response approximation of the VCO's dynamic frequency, Eq. (4), becomes inaccurate

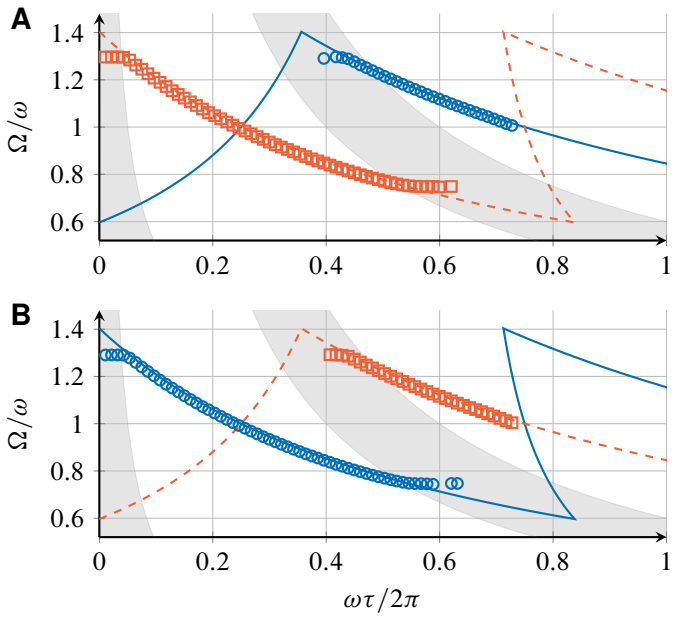

Fig. 5: Collective frequency Ω of the in-phase (blue circles) and anti-phase synchronized state (red squares) for two mutually coupled DPLLs as a function of the transmission delay τ. Symbols show experimental data points. Lines show analytical results of the phase model, Eq. (8), where solid blue lines denote in-phase solutions and dashed red lines denote anti-phase solutions. The shaded areas display the VCO clipping region. (A) Operation mode with signal inverter deactivated. (B) Operation mode with signal inverter activated.

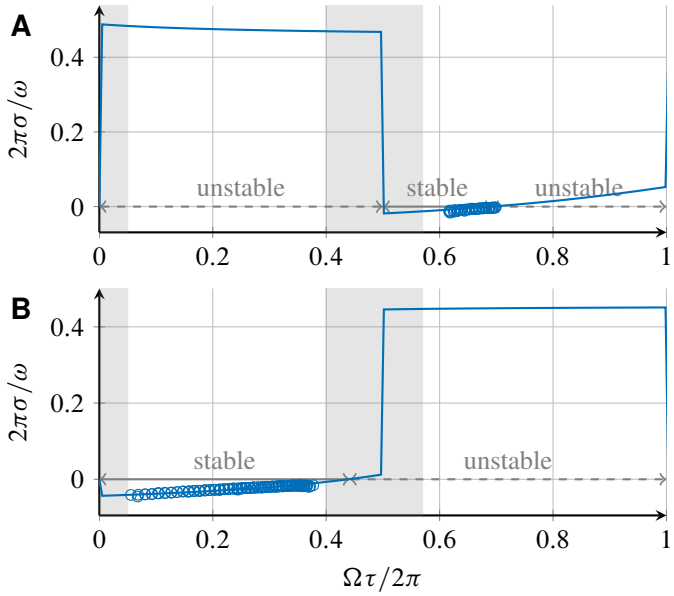

Fig. 6: Perturbation response rate σ, Eq. (13), of the in-phase synchronized state for a system of two mutually coupled DPLLs for (A) deactivated inverter and (B) activated inverter. Symbols show experimental data points. Lines show results of the phase model, numerical solutions to Eq. (15) with $\zeta = -1$. The shaded areas display the VCO clipping region.

(Fig. 2). Hence, the measured collective frequency deviates from the theoretical results. The value of the coupling delay determines whether only one or multiple solutions are stable. In addition, switching the activation state of the signal inverter in the feedback loop (see Fig. 1) exchanges the collective frequency and the stability of the in-phase and the anti-phase synchronized state (see Fig. 5B).

From experimental measurements, we obtained the exponential relaxation time of the phase difference between the two DPLLs, which corresponds to the perturbation response rate σ from the phase model, Eq. (13). The experimental and theoretical results for the perturbation response rate are shown in Fig. 6. Experimental data were obtained outside the VCO clipping regions and for values of the delay for which the in-phase synchronized state is stable ($\sigma < 0$). Again, the experimental results are in excellent agreement with the results from the phase model. Moreover, the perturbation response rate is a non-monotonic function of the coupling delay and displays local extrema suitable for efficient operation.

V. Discussion

In this paper, we have shown theoretically and experimentally that global synchronization can be achieved in mutually delay-coupled systems of DPLLs. We developed a theory of coupled phase oscillators taking into account the effects of filtering and transmission delays. We obtained analytical results for the collective frequency of the in-phase synchronized state and analyzed its stability. We showed how the collective frequency as well as the time scales of synchronization depend on the characteristics of the DPLLs' filters and on transmission delays. Specifically, the collective frequency of the synchronized state in general differs from the intrinsic frequency of the DPLLs. Moreover, it does not depend on the total number of oscillators and the details of the coupling topology. Hence, our approach of mutually coupled distributed DPLLs can scale up to massive MIMO systems with an arbitrary number of oscillators. We believe that our approach is particularly relevant for massive MIMO due to considerable delays induced by typical spacing between antennas. However, it can also be applied to other problems where a large number of electronic clocks have to be synchronized.

We designed experiments to test the predictions of our phase model in real systems of coupled DPLLs. Our measurements of the collective frequency and the synchronization speed show mostly excellent quantitative agreement with the theoretical results. Deviations of experimental and theoretical results only occur at the stability boundaries and are due to the idealized description of the VCO response in the phase model. These proof-of-concept experimental results are the first step to demonstrate the viability of our approach for technical applications.

For massive MIMO systems, our results suggest that mutually delay-coupled DPLLs are a viable way to synchronize the carrier frequencies of large numbers of antennas. In contrast to master clock architectures, such mutually coupled systems are highly scalable and simple to implement. In addition, such architectures limit energetic costs of signal amplification requiring only short wiring distances. The theory presented here is a practical tool to identify system parameters required for the desired application.

With an increasing number of mutually delay-coupled DPLLs in the network, more and more dynamical states become possible in addition to in-phase synchronized state. A possible strategy to boot the system into global synchrony is to first synchronize a subnetwork of two DPLLs and sequentially connecting the remaining DPLLs of the network once the subnetworks are synchronized. The problem of efficiently booting such systems into synchrony is an interesting topic for future research.

Appendix

The Fourier representation of the square wave function Π and the triangle function Δ are given by

$$\Pi(\phi) = \frac{1}{2} + \frac{2}{\pi}\sum_{i=0}^{\infty}\frac{\sin(a_i\phi)}{a_i} \ , \tag{16}$$

$$\Delta(\phi) = -\frac{8}{\pi^2}\sum_{i=0}^{\infty}\frac{\cos(a_i\phi)}{a_i^2} \ , \tag{17}$$

where $a_i = 2i + 1$. Hence evaluating Eq. (2) yields,

$$\begin{aligned} x_k^{\mathrm{PD}} &= \frac{1}{2} - \frac{8}{\pi^2}\sum_{ij}\frac{\sin(a_i\phi_{l,\tau})\sin(a_j\phi_k)}{a_i a_j} \\ &= \frac{1}{2} - \frac{4}{\pi^2}\sum_{i}\frac{\cos(a_i(\phi_{l,\tau}-\phi_k))}{a_i^2} \\ &\quad - \frac{4}{\pi^2}\sum_{i\neq j}\frac{\cos(a_i\phi_{l,\tau}-a_j\phi_k)}{a_i a_j} \\ &\quad - \frac{4}{\pi^2}\sum_{ij}\frac{\cos(a_i\phi_{l,\tau}+a_j\phi_k)}{a_i a_j} \ , \end{aligned} \tag{18}$$

where $\phi_{l,\tau}(t) = \phi_l(t-\tau)$. The different sums in the second identity represent different frequency components. From Eq. (4), it can be seen that $\dot{\phi}_k - \dot{\phi}_l = \mathcal{O}(K_{\mathrm{VCO}})$. Hence, the first sum in the second identity contains low frequency components. The lowest frequency components in the second sum are given by the terms with $i + j = 1$. From Eq. (4), it can be seen that $a_i\dot{\phi}_k - a_{1-i}\dot{\phi}_l = \mathcal{O}(2\omega_0)$ for $i \in \{0,1\}$ and hence, the second sum contains only high frequency components. The lowest frequency component in the third sum is given by the term with $i = j = 0$. From Eq. (4), it can be seen that $\dot{\phi}_k + \dot{\phi}_l = \mathcal{O}(2\omega_0)$ and hence, the third sum contains only high frequency components. Thus, using Eq. (17), we can write x_k^{PD} as

$$x_k^{\mathrm{PD}}(t) = \frac{1}{2} + \frac{1}{2}\Delta\big(\phi_l(t-\tau) - \phi_k(t)\big) + R_{\mathrm{HF}}(t) \ , \tag{19}$$

where R_{HF} denotes the high frequency components of the signal. In Eq. (5), we approximate $\int_0^\infty \mathrm{d}u\ p(u)R_{\mathrm{HF}}(t-u) \simeq 0$, assuming ideal suppression of the high frequency components by the loop filter [17].

Acknowledgment

This work is partly supported by the German Research Foundation (DFG) within the Cluster of Excellence 'Center for Advancing Electronics Dresden'.

REFERENCES

[1] E. Dahlman, S. Parkvall, J. Skold, and P. Beming, *3G Evolution : HSPA and LTE for Mobile Broadband*. Elsevier Science, 2010.

[2] M. Gast, *802.11n: A Survival Guide*. O'Reilly Media, 2012.

[3] L. Lu, G. Y. Li, A. L. Swindlehurst, A. Ashikhmin, and R. Zhang, "An Overview of Massive MIMO: Benefits and Challenges," *Selected Topics in Signal Processing, IEEE Journal of*, vol. 8, no. 5, pp. 742–758, Oct 2014.

[4] F. Rusek, D. Persson, B. K. Lau, E. Larsson, T. Marzetta, O. Edfors, and F. Tufvesson, "Scaling Up MIMO: Opportunities and Challenges with Very Large Arrays," *Signal Processing Magazine, IEEE*, vol. 30, no. 1, pp. 40–60, Jan 2013.

[5] E. Larsson, O. Edfors, F. Tufvesson, and T. Marzetta, "Massive MIMO for next generation wireless systems," *Communications Magazine, IEEE*, vol. 52, no. 2, pp. 186–195, February 2014.

[6] D. Rahn, M. Cavin, F. Dai, N. H. W. Fong, R. Griffith, J. Macedo, A. Moore, J. Rogers, and M. Toner, "A fully integrated multiband MIMO WLAN transceiver RFIC," *Solid-State Circuits, IEEE Journal of*, vol. 40, no. 8, pp. 1629–1641, Aug 2005.

[7] V. Rabinovich and N. Alexandrov, *Antenna Arrays and Automotive Applications*. Springer, 2012.

[8] T. Schenk, *RF Imperfections in High-rate Wireless Systems. Impact and Digital Compensation*. Springer, 2008.

[9] A. Pitarokoilis, S. Mohammed, and E. Larsson, "Uplink Performance of Time-Reversal MRC in Massive MIMO Systems Subject to Phase Noise," *Wireless Communications, IEEE Transactions on*, vol. 14, no. 2, pp. 711–723, Feb 2015.

[10] C. Shepard, H. Yu, N. Anand, E. Li, T. Marzetta, R. Yang, and L. Zhong, "Argos: Practical many-antenna base stations," in *Proceedings of the 18th Annual International Conference on Mobile Computing and Networking*, ser. Mobicom '12. New York, NY, USA: ACM, 2012, pp. 53–64.

[11] R. Ho, K. Mai, and M. Horowitz, "The future of wires," *Proceedings of the IEEE*, vol. 89, no. 4, pp. 490–504, 2001.

[12] E. Mensink, D. Schinkel, E. Klumperink, E. Van Tuijl, and B. Nauta, "Power Efficient Gigabit Communication Over Capacitively Driven RC-Limited On-Chip Interconnects," *Solid-State Circuits, IEEE Journal of*, vol. 45, no. 2, pp. 447–457, 2010.

[13] S. Strogatz, *Sync: The Emerging Science of Spontaneous Order*, ser. Penguin Press Science Series. Penguin, 2004.

[14] S. H. Strogatz, "From Kuramoto to Crawford: exploring the onset of synchronization in populations of coupled oscillators," *Physica D: Nonlinear Phenomena*, vol. 143, no. 1-4, pp. 1–20, 2000.

[15] A. C. Oates, L. G. Morelli, and S. Ares, "Patterning embryos with oscillations: structure, function and dynamics of the vertebrate segmentation clock," *Development*, vol. 139, no. 4, pp. 625–639, 2012.

[16] A. Pollakis, L. Wetzel, D. J. Jörg, W. Rave, G. Fettweis, and F. Jülicher, "Synchronization in Networks of Mutually Delay-Coupled Phase-Locked Loops," *New Journal of Physics*, vol. 16, no. 11, p. 113009, 2014.

[17] F. M. Gardner, *Phaselock Techniques*. Wiley, 2005.

[18] S. H. Strogatz, *Nonlinear Dynamics And Chaos: With Applications to Physics, Biology, Chemistry and Engineering*. Westview Press, 2008.

[19] A. Amann, E. Schöll, and W. Just, "Some basic remarks on eigenmode expansions of time-delay dynamics," *Physica A: Statistical Mechanics and its Applications*, vol. 373, pp. 191–202, Jan. 2007.

[20] R. Mancini, *Op Amps for Everyone: Design Reference*. Newnes, 2003.

[21] Texas Instruments, "CD4046B CMOS Micropower Phase-Locked Loop," http://www.ti.com/product/cd4046b, accessed: 2014-09-24.

[22] Digilent Inc., "chipKIT Max32 reference manual," http://www.digilentinc.com/Products/Detail.cfm?Prod=CHIPKIT-MAX32, accessed: 2014-09-22.

[23] Pico Technology, "PicoScope 2205 Mixed–Signal Oscilloscope," http://www.picotech.com/mixed-signal-oscilloscope.html, accessed: 2014-09-22.